AIAA JOURNAL
Vol. 35, No. 4, April 1997

OH Planar Laser-Induced Fluorescence Velocity Measurements in a Supersonic Combustor

G. Gauba,* K. G. Klavuhn,* J. C. McDaniel,† K. G. Victor,* R. H. Krauss,‡ and R. B. Whitehurst III§
University of Virginia, Charlottesville, Virginia 22903

Quantitative velocity measurements have been made in a hydrogen/air reacting flow in a supersonic combustor model. These measurements were made with an unswept ramp fuel injector in a clean-air, electrically heated supersonic combustion tunnel. A nonintrusive optical velocity measurement technique based on OH planar laser-induced fluorescence (OH PLIF) has been used for this study. A narrow line-width, tunable, pulse-amplified, doubled-dye uv beam was used to resolve an OH spectral line by monitoring the laser-induced fluorescence at every point in the measurement plane. The Doppler-shifted line center was measured with a counterpropagating scheme to eliminate collisional impact shifts. Velocity fields were measured in five planes parallel to the injector wall. The maximum streamwise component is 700–800 m/s and the transverse spreading component is much smaller compared to the streamwise component. These measurements have an uncertainty of ±6–8% in flow regions with the maximum velocity. The spatial resolution and accuracy of these measurements provide a unique benchmark data set (which also includes OH PLIF absolute concentration and temperature) for computational fluid dynamics validation of reacting supersonic combustion flows.

Introduction

THE need for easier and more economic access to space, as well as the desire for higher-speed civil aircraft, motivated a resurgence of interest in hypersonic flight in the 1980s. The proposed concept in the United States for a single-stage-to-orbit hypersonic flight vehicle, the National Aerospace Plane (NASP), utilizes an air-breathing propulsion system with the engine completely integrated into the airframe. These engines burn air and fuel at supersonic speeds to eliminate the losses associated with subsonic combustion at hypersonic flight Mach numbers.

Because the combustor inlet speeds are on the order of 1 km/s and combustor lengths on the order of 1 m, the residence time in the supersonic combustor is very short, on the order of 1 ms. As a result, rapid mixing of fuel and air and fast chemical kinetics are required to achieve efficient combustion. Fuel can be injected either perpendicular or parallel to the main airflow. In this investigation, the injected jet is oriented at a 10-deg angle relative to the main air flowfield and the injection is primarily parallel to the main airflow; the slight transverse component helps in jet penetration into the main airflow. This is referred to as a parallel injection scheme[1] for the current investigation. Parallel injection offers lower losses and, in fact, augments thrust by adding the fuel momentum to that of the main airstream.

Parallel injection, however, suffers from lower mixing efficiency—a problem that becomes more severe with increasing Mach number. To enhance air–fuel mixing, hydrogen is injected from the base of an unswept ramp injector.[1] The ramp geometry is such that the ramp sides are parallel to the main airflow. The basic purpose of the ramp is to provide a source of vorticity, which interacts with the injected hydrogen jet to enhance fuel–air mixing.[2] An additional function of the ramp geometry is to provide a subsonic recirculation region, which serves as the flame-holding region. A schematic representation of the major flow features of an unswept ramp injector used in the study reported here is presented in Fig. 1. As shown in this figure, the flowfield is very complex, involving subsonic recirculation regions, three-dimensional shocks, and shock/boundary-layer interactions.

Experimental generation of the high-enthalpy conditions that occur in the NASP supersonic combustion ramjet (scramjet) during flight is a challenging task.[3] Considering the limitations of ground-based facilities, numerical simulations offer the only alternative for thorough parametric examination of these complex internal flows. However, keeping the complexity of these flows in mind, the numerical simulations need to be compared with experimental results at representative experimental conditions. After sufficient validation, the computational fluid dynamics (CFD) simulations become an important design tool.

An electrically heated supersonic combustion tunnel[4] and the associated laser diagnostics facilities at the University of Virginia's Aerospace Research Laboratory provide the capability to generate experimental data for CFD validation of reacting combustor flowfields. The objective of the current study is to apply OH planar laser-induced fluorescence (PLIF) velocimetry to provide detailed, spatially-resolved, and time-averaged velocity measurements with sufficient accuracy for CFD validation in the reacting combustor flowfield.

OH PLIF Velocimetry

A variety of techniques are available for velocity field measurements. Some of these techniques are based on the introduction of particles into a flow, such as particle image velocimetry[5] and digital image velocimetry.[6] These techniques have been applied with great success to low-speed incompressible flows. Attempts have also been made to extend these techniques to high-speed flows; however, in the very high speed flows, the particle-based methods have a problem with particle tracking in large gradient regions of the flow. However, CFD simulations provide sufficient information to evaluate the particle trajectories[7] and compare the simulations with the measured velocity fields.

In the current study, velocity is measured by recording Doppler-shifted OH LIF. For reacting flows, OH radicals are a naturally occurring combustion intermediate species, with spectral absorption lines that are accessible with currently available uv lasers. OH LIF velocimetry can be applied for accurate velocity measurement in high-speed reacting flows because this technique does not suffer from particle-tracking problems. Also, no extraneous material is introduced into the flow, so there is no concern about altering the chemical kinetics of the reacting flow. This technique has been successfully demonstrated and validated in a reacting underexpanded jet flowfield.[8,9]

Received Feb. 18, 1995; revision received Dec. 2, 1996; accepted for publication Dec. 24, 1996.

*Graduate Research Assistant, Aerospace Research Laboratory, Department of Mechanical, Aerospace, and Nuclear Engineering. Member AIAA.
†Professor, Aerospace Research Laboratory, Department of Mechanical, Aerospace, and Nuclear Engineering. Member AIAA.
‡Research Associate Professor, Aerospace Research Laboratory, Department of Mechanical, Aerospace, and Nuclear Engineering. Member AIAA.
§Research Scientist, Aerospace Research Laboratory Department of Mechanical, Aerospace, and Nuclear Engineering. Member AIAA.

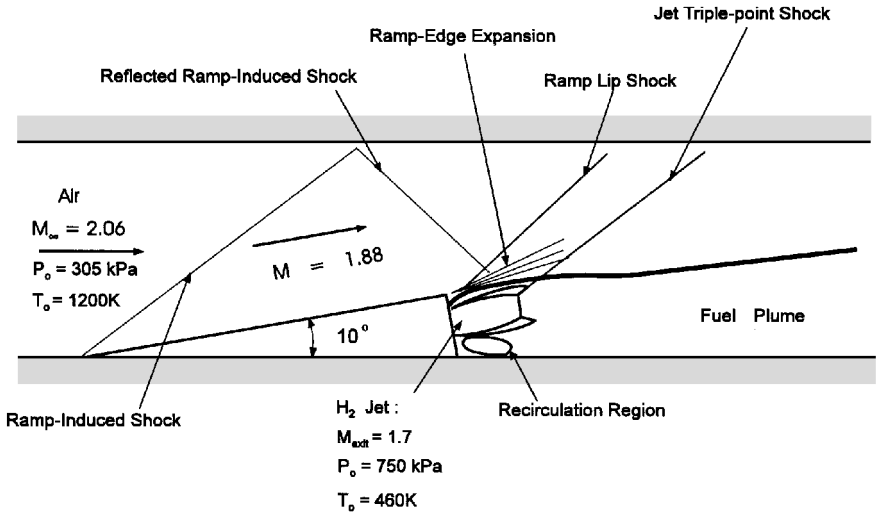

Fig. 1 Schematic illustration of nonreacting flow features for parallel injection using an unswept ramp injector.

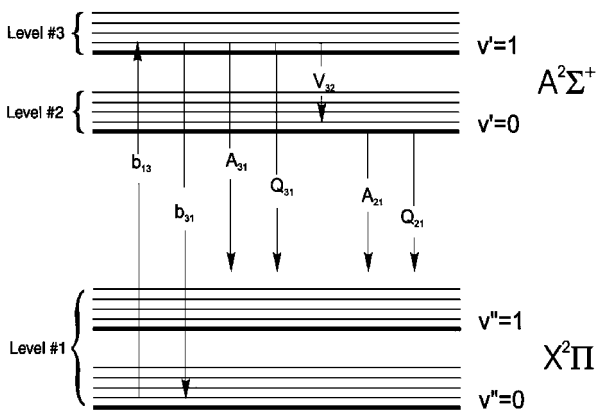

Fig. 2 Excitation and emission model for OH LIF.

OH LIF

In the current study, an OH transition between the $X^2\Pi$ ground state and $A^2\Sigma^+$ excited electronic state is used for LIF measurements. A schematic representation of the excitation and emission model is presented in Fig. 2. The incident radiation induces a transition (b_{13}) from the $v'' = 0$ ground electronic state (level 1) to a rotational level in the $v' = 1$ excited electronic state (level 3). The excited molecules decay back to the ground state through spontaneous emission (A_{31}), stimulated emission (b_{31}), collisional transfer (V_{32}), or collisional quenching (Q_{31}). The LIF signal (A_{31} and A_{21}) is collected both during and after the laser-pulse duration. A detailed modeling of the LIF signal has been presented in Ref. 8.

The (1, 0) vibrational excitation band offers a number of advantages. This band has a large absorption coefficient, which facilitates planar measurements by providing a sufficiently high signal. This band also facilitates LIF detection because of significant spectral separation from the strong radiation associated with the (1, 1) and (0, 0) bands. The Q rotational branch in the (1, 0) vibrational transition has been used in the current study. Of the various rotational transitions, Q(5) is chosen because it has a significant Boltzmann population fraction in the temperature range of interest and because it is located in a sufficiently isolated spectral region. To reduce absorption effects, the satellite $Q_{21}(5)$ transition is chosen for LIF velocity measurements.

Velocimetry Technique

The basis of the velocity measurement technique is measurement of the Doppler frequency shift by using counterpropagating laser sheets to cancel the additional collisional impact shift; it is illustrated in Fig. 3. A laser sheet is passed through the flow at a suitable angle θ_i and LIF images are recorded as a function of laser frequency. Subsequent to this series of images the sheet is passed through the flow 180 deg to the first direction. Because the Doppler shifts for the two counterpropagating directions differ only by the sign and because the impact shifts are the same for these two counterpropagating directions, the following equations result for the measured Doppler shifts along the i, $i\prime$ direction:

$$\Delta\nu_{d_{i,i\prime}} = \frac{\Delta\nu_i - \Delta\nu_{i\prime}}{2} = \frac{(\Delta\nu_{d_i} + \Delta\nu_I) - (\Delta\nu_{d_{i\prime}} + \Delta\nu_I)}{2} \tag{1}$$

$$\Delta\nu_{d_{i,i\prime}} = \frac{\Delta\nu_{d_i} - \Delta\nu_{d_{i\prime}}}{2} = \frac{\Delta\nu_{d_{i,i\prime}} - \Delta\nu_{d_{i\prime,i}}}{2} \tag{2}$$

In these equations, $\Delta\nu_i$ is the total frequency shift along direction i, $\Delta\nu_{d_i}$ is the Doppler shift along direction i, and $\Delta\nu_I$ is the impact shift. The frequency difference between the measured line centers is twice the Doppler shift. The primary advantage of this counterpropagating measurement scheme is that it eliminates other sources of line-center shift, such as impact or collisional shift. A secondary advantage of this measurement scheme is that it eliminates systematic errors due to factors such as spectral broadening and nonsymmetric line shapes. This measurement must be repeated with the beam oriented at a different angle to measure both velocity components within the plane.

Using the basic relation between the measured Doppler shift and the velocity component,

$$\Delta\nu_d = \boldsymbol{k} \cdot \boldsymbol{u}/2\pi \tag{3}$$

and solving for u_x and u_y in the flowfield coordinates gives the desired velocity components as a function of $u_{i,i\prime}$, $u_{j,j\prime}$, $\theta_{i,i\prime}$, $\theta_{j,j\prime}$. For a symmetric flow, it is possible to eliminate one direction and still be able to calculate the entire velocity field.[8] This method is illustrated in Fig. 3. For a symmetric flow, the velocity vectors are such that at corresponding points across the symmetry plane the following relationships hold:

$$u_{1x} = u_{2x} \tag{4}$$

$$u_{1y} = -u_{2y} \tag{5}$$

Consider two directions, i and j, oriented so that $\theta_j = \theta_i + 90$ deg. The projected velocities along directions follow the relationship

$$u_{1j} = -u_{2i} \tag{6}$$

$$-u_{1i} = u_{2j} \tag{7}$$

After measuring u_{1i} and u_{2i}, Eqs. (6) and (7) allow u_{1j} and u_{2j} to be calculated. At this stage, the information for projected velocity along

two directions has been determined. The velocities in the flowfield (x, y) coordinate system can now be evaluated from the following relations:

$$u_{1x} = \_u_{1i} \cos\theta_i \_ u_{1j} \cos\theta_j \quad (8)$$

$$u_{1y} = \_u_{1i} \sin\theta_i + u_{1j} \sin\theta_j \quad (9)$$

Experimental Setup

Combustion Tunnel

These experiments were conducted in a supersonic combustion wind tunnel. This facility is designed for continuous, steady-state operation limited to several hours only by fuel supply. The ability to sustain combustion for long periods is an absolute necessity for the OH PLIF velocity measurement currently reported because it is a time-intensive process, requiring the collection of a large number of images to resolve the entire OH spectral line from each of the flow directions shown in Fig. 3. The supersonic combustion tunnel currently provides a flow with a test-section static pressure from 37 kPa ($\frac{3}{8}$ atm) to 50 kPa ($\frac{1}{2}$ atm) with a stagnation temperature up to 1200 K. Details of the combustion tunnel design and performance characteristics have been reported previously.[4,10,11] The flow conditions for the current study are given in Table 1.

As a routine part of the combustion tunnel experiments, wall pressures and temperatures were recorded, along with many other operational conditions. Another PLIF approach using a KrF laser, provided planar OH temperature and density measurements for this flowfield.[12,13]

Table 1 Supersonic combustion tunnel operational parameters

Parameter	Tunnel (air)	Injector (H_2)
P_0, kPa	305	750
T_0, K	1200	460
Mach number	2.06 (freestream)	1.7 (exit)
P_∞, kPa	37	149
T_∞, K	695	290
U_∞, m/s	1060	2218
Mass flow rate	0.19 kg/s	1.41 g/s

Dimensions of the test section, unswept ramp geometry, and a reference axis system are presented in Fig. 4. The tunnel test section starts with a replaceable injector block. For the current work, an unswept ramp injector block has been used. The top surface of the ramp is inclined at a 10-deg angle to the base wall and the injector face is perpendicular to the top surface. The ramp height (H) is 6.35 mm (0.25 in.) and the ramp width is twice the height. A 2.54-mm (0.1 in.) diameter (D) circular injector is located on the injector face. Both these dimensions are used as a reference scale with $H = 2.5\ D$.

Initially, the test section is a uniform duct with a rectangular cross section $6H$ wide and $4H$ high. The uniform part of the test section extends to a location $10H$ downstream of the injector base. At $X/H = 10$ the tunnel base wall has a 2.9-deg divergence. The tunnel test section has glass windows on three sides that allow optical access to the flow. These windows are mounted on the front wall (on the side opposite the unswept ramp base) and the two side walls (on either side of the unswept ramp). In the present study, a laser sheet is transmitted through each side window and the LIF is recorded by a charge-coupled device (CCD) camera viewing in through the front window.

Laser System

To conduct accurate OH PLIF measurements using the Doppler shift, a narrow linewidth, tunable, pulse-amplified uv laser source is required. A complex system using a number of lasers is required to generate the desired beam characteristics. This system was developed, tested, and calibrated for a reacting underexpanded jet and has been previously described by Klavuhn et al.[9]; however, a brief description is presented below. The system consists of an argon ion laser, producing 4-W single-line output at 514.4 nm, to pump a ring dye laser. The ring dye generates a narrow-linewidth, tunable beam with 450 mW at 566 nm and with a linewidth of $\sim$20 MHz. A fraction of the beam is split off and passed through a frequency stabilizer. The frequency stabilizer is critical for single-mode lasing of the ring dye in a noisy environment with long operating times at a desired frequency. A small fraction of this beam is also split off to monitor absolute and relative laser frequency information with a wave meter, spectrum analyzer, and an I_2 static cell. The remaining portion of the beam is transmitted into a pulsed dye amplifier (PDA), pumped by a Nd:YAG laser. The output of the PDA is an amplified, 10-ns duration, pulsed beam at 566 nm, with 40 mJ per pulse.

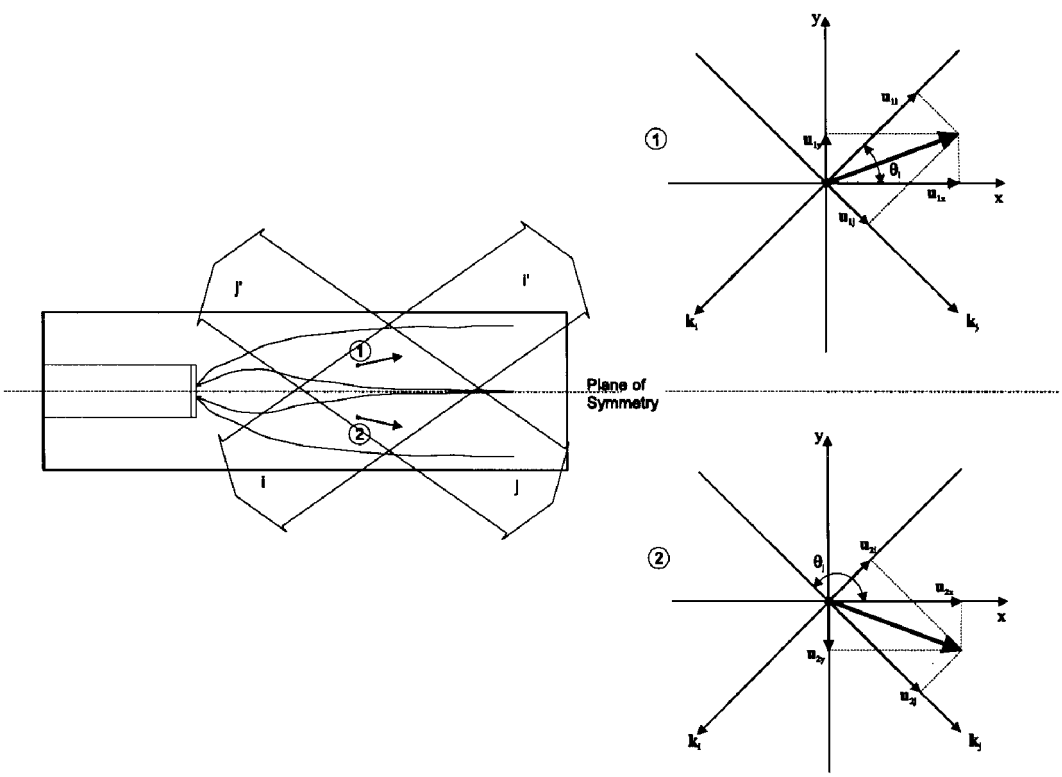

Fig. 3 Velocity measurement scheme for a flow with symmetry.

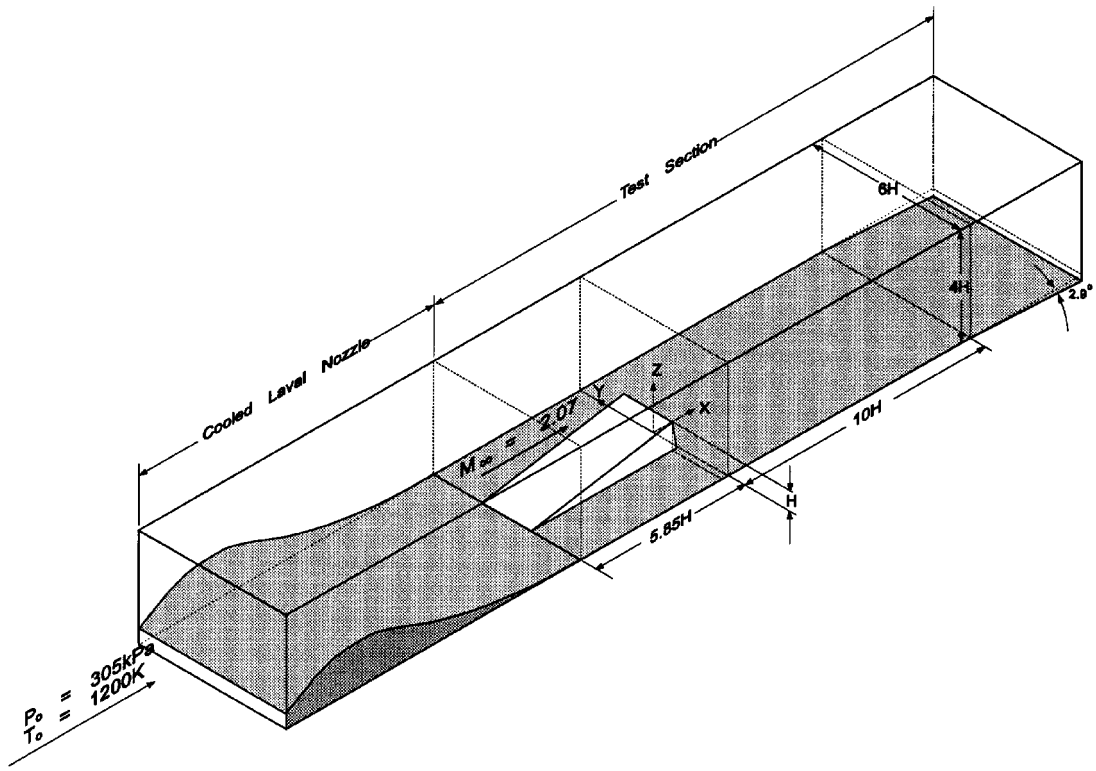

Fig. 4 Major dimensions of the tunnel test section and the unswept ramp injector.

This beam is passed through a wavelength doubler to produce a uv laser beam at 283 nm with 1.5–2.2 mJ per pulse. The laser beam is passed into the combustion tunnel room and through sheet-forming optics. The beam is spread in one dimension by passing it through a $f = 50$ mm cylindrical lens and then collimated by transmitting it through a $f = 300$ mm spherical lens. This lens combination produces a sheet approximately 300 μm thick and 25 mm wide. For the counterpropagating measurement technique a laser sheet has to be transmitted through the flow from either side of the tunnel. The sheet-forming optics is mounted on optical rails on both sides of the tunnel test section. A mirror mounted on a precise positioning (Klinger) stage can be moved in and out of the incident laser beam to select either of the optical rails. These two optical rails are connected to a common frame and this optical assembly is mounted on another Klinger translational stage. This translational stage allows the laser sheet to be positioned at a desired Z/H location with a nominal accuracy of 1 μm. The CCD camera is mounted on a separate translation stage and when required it is moved by the same distance as that traversed by the laser sheet.

Procedure

The ring dye laser is controlled by a laboratory 486 PC that is used to scan the laser through a 16-GHz frequency range. For each scan, 800 data points with a separation of 20 MHz are recorded. At each frequency location, information about absolute and relative frequency location are recorded. Absolute frequency location is determined by recording a reference I_2 static cell fluorescence. Relative frequency information is collected from a 2-GHz interferometer. Because an OH spectral linewidth is on the order of a few gigahertz, it is possible to resolve the OH spectral line with a frequency resolution lower than that required to resolve the reference I_2 spectra and interferometer fringes. So an OH PLIF image is recorded at an interval of 25 points, giving a set of 32 images for every frequency scan.

The laser frequency scan is paused every 500 MHz to allow a signal to be sent to a Princeton Instruments gated, intensified CCD camera to collect an OH PLIF image. The camera collects the fluorescence signal for 4 s. Each image is stored on a laboratory 486 PC that is dedicated to camera control and image acquisition. Each scan takes approximately 5 min, and it takes approximately 45 min to collect three complete sets of redundant measurements for each plane. These images are later transferred to an RS6000 workstation and the OH spectral line is extracted for each camera pixel. The procedure for reconstructing the spectrum for any pixel is illustrated in Fig. 5. The signal value at a given pixel is extracted from each of the 32 images to reconstruct the entire line shape at the corresponding point in the flowfield. The line center location is determined by fitting a Lorentzian function to the data. Subsequently, the Doppler shifts are determined and the velocities are calculated by Eqs. (1–5).

Results and Discussion

Velocity measurements have been made for five planes oriented parallel to the base of the injector ramp located on the lower tunnel wall (see Fig. 6). These planes were selected to illustrate the transverse spreading of the injected hydrogen. It can be seen in Fig. 6 that these planes are located at the injector center and at $\pm 1D$, $+0.5D$, $+1D$, $+2D$ relative to the injector center, where D is the injector exit diameter. This figure also shows the measurement region for OH number density and temperature measurements[13] obtained in a separate investigation. As previously mentioned, complete velocity information can be extracted only in the overlap region between the two independent orientations of the doubled-dye laser sheet. This overlap region, shown as the diamond-shaped region (bold outline) in Fig. 6, extends from 4 to 10 ramp heights (10–25D) downstream of the ramp injector face and ± 2.5 ramp heights around the tunnel center line.

A set of raw fluorescence images in measurement planes located at $Z/D = \pm 1.0$, 0.0, $+1.0$, and $+2.0$ is presented in Fig. 7. These images are a typical sample picked at random from the three data sets collected. Each image set shows similar spatial fluorescence distribution, and this is a measure of the repeatability of the fluorescence signal. It is evident that the strongest signal occurs in two dominant lobes, which are also observed in a chemiluminescence image (presented later). As expected, the signal variation in the downstream direction within each lobe is primarily due to intensity variations in the laser sheet. A plot of the normalized sheet intensity profile is also presented in Fig. 7. This profile was measured by

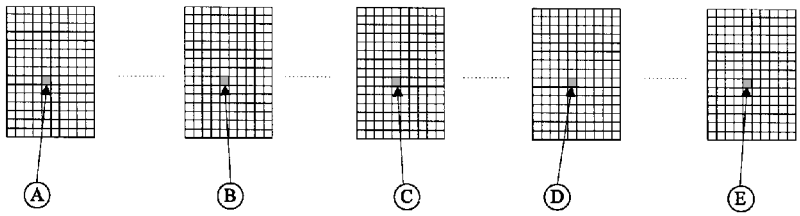

Series of 32 PLIF images at different frequencies

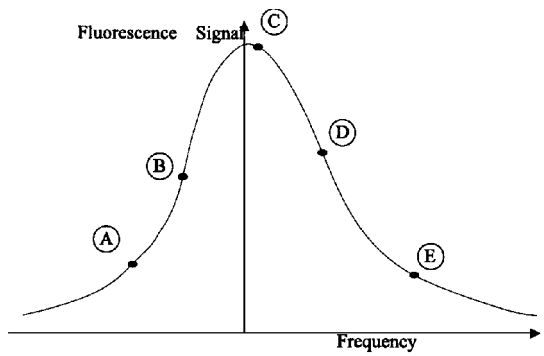

Extract signal values for same pixel location and plot vs frequency

Fig. 5 Illustration of the procedure to reconstruct the spectrum at any point from a series of fluorescence images.

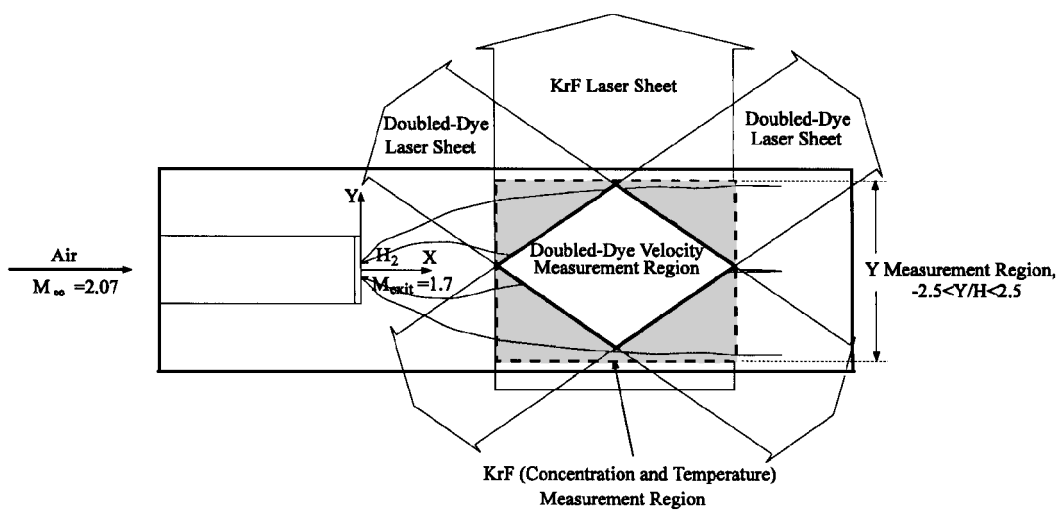

a) Top view

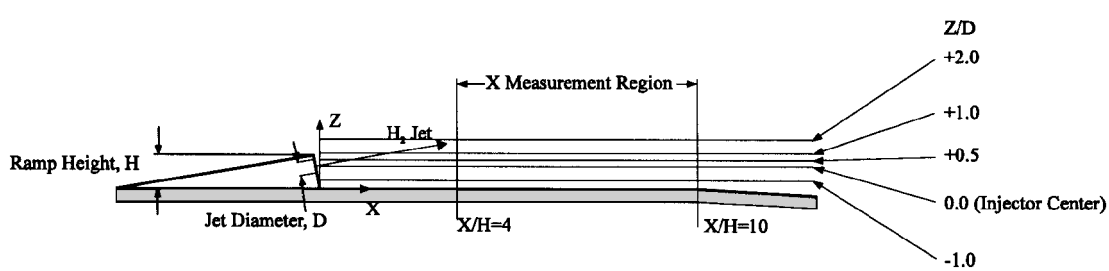

b) Side view

Fig. 6 Location of measurement regions in supersonic combustion tunnel test section.

recording an image of the incident laser sheet on a plate of ground glass.

The signal in the flow center is significantly lower than that observed in the two lobes. The plane $Z/D = \pm 1.0$ shows more uniform signal distribution compared to the plane $Z/D = 0.0$. This is consistent with the fact that the plane $Z/D = \pm 1.0$ is located below the injected jet and it is expected that recirculation regions would uniformly mix the available OH. The planes, $Z/D = +1.0$ and $+2.0$, show a decreasing amount of signal in the center of the flow. This is consistent with the expected fuel-plume structure, where the reactions occur in a shell at the outer limits of the plume. No measurements were made beyond $Z/D = 2.0$ because of a decreased OH LIF signal in the flow center with increasing Z/D.

A sample set of spectra obtained from both the counterpropagating directions on either side of the tunnel center line are presented in Fig. 8. These spectra are extracted from the points $X/H = 8.31$, $Y/H = 1.79$ and $X/H = 5.81$, $Y/H = \pm 1.91$. These points are located on the laser-sheet path at approximately the same distance around the center line. These spectra show no significant differences between the points that are located near the entrance and exit of the

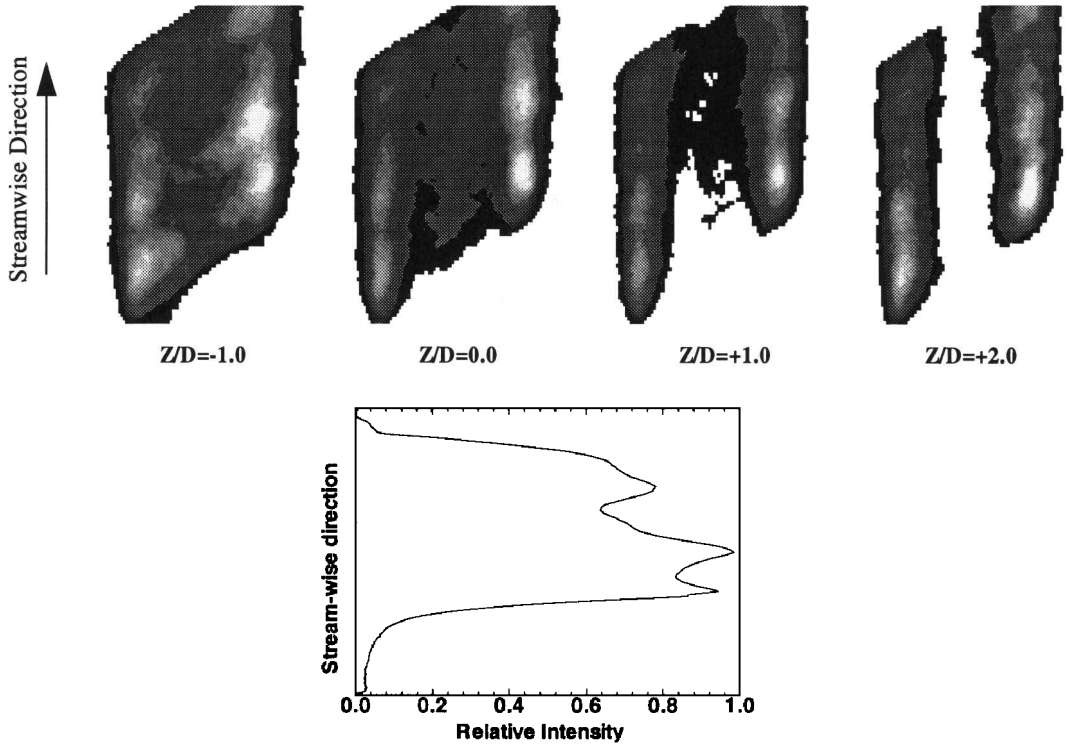

Fig. 7 Signal distribution variation across the measurement planes.

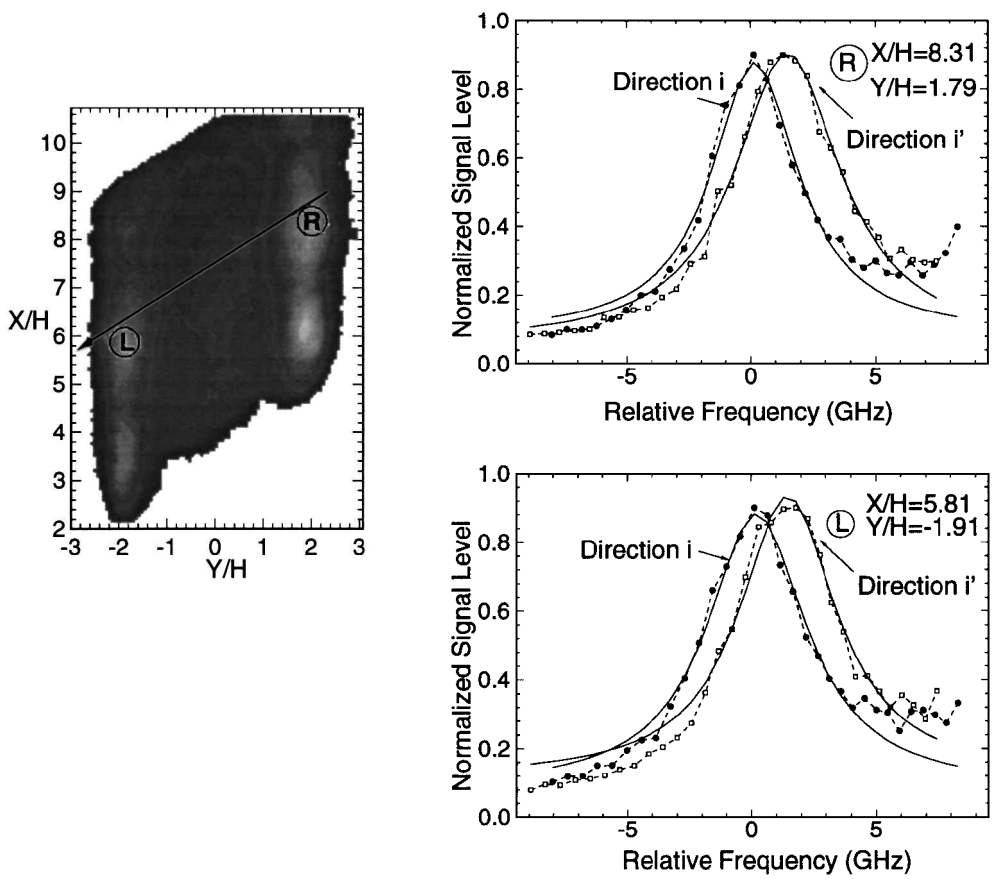

Fig. 8 Sample spectra obtained from each of the counterpropagating directions for two locations on either side of the tunnel center line.

laser sheet into the flow. Because three redundant data sets were collected for each direction, a measure of the repeatability of the data can be obtained by examining the absorption line center. The center of the absorption line is determined by curve fitting a Lorentzian profile to the data and for the point shown in Fig. 8, $X/H = 8.31$, $Y/H = 1.79$, along direction ii, the center line frequency is determined to be 1.43, 1.42, and 1.39 GHz. The curve-fit procedure minimizes goodness of fit χ^2 for the spectrum at each location. The major factor contributing to the curve-fit uncertainty and eventually the velocity uncertainty, is the intermittency of the OH signal in the turbulent reacting flow. However, for any pixel, the signal fluctuations will affect the images at each frequency in a similar manner. This effect can be reduced by collecting a LIF signal for a statistically significant number of laser shots, which is not practical to implement. The velocity uncertainty due to this and other factors can then be estimated[8] provided that the signal-to-noise ratio, Lorentzian width ($\Delta\nu_l$), and number of points are known. The measured velocity uncertainty is estimated after the above parameters are determined during the curve-fit procedure.

For the results presented here, flow symmetry has been assumed to generate the velocity fields. For flows with symmetry, it is possible to reduce the required data sets from four to two. This advantage allows more measurements to be made to generate more complete flow mapping. It has previously been shown in underexpanded reacting jets that measurements made with this assumption compare very well with measurements made without assuming symmetry.[8]

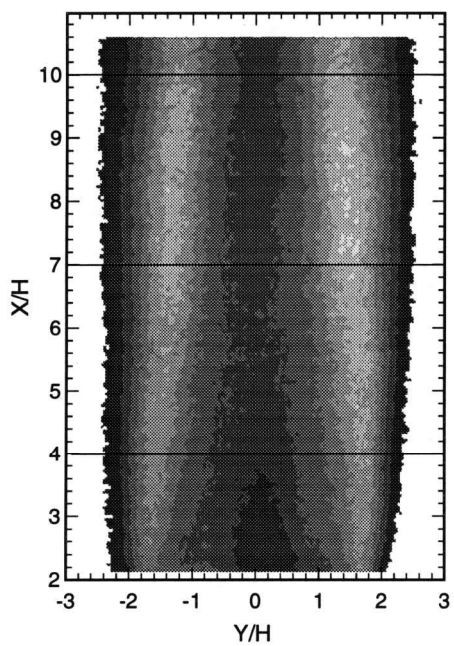

Fig. 9a Chemiluminescence image of the measurement region for the test-section flow.

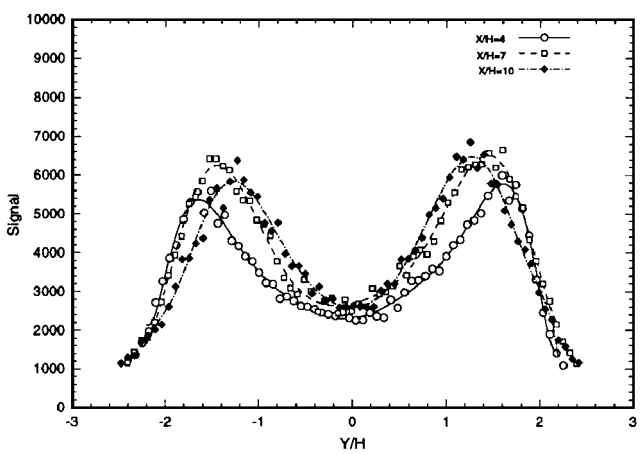

Fig. 9b Signal intensity variation across the image at three different axial locations X/H = 4, 7, and 10.

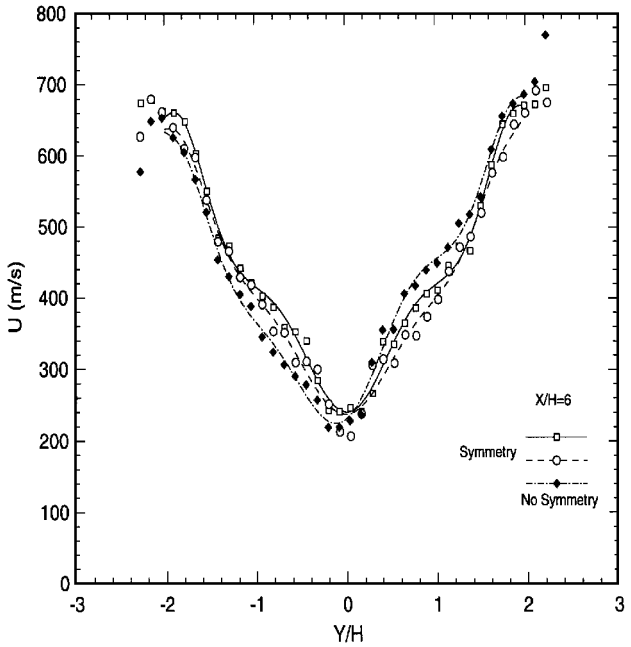

Fig. 10 Transverse velocity profile at $Z/D = \pm 1.0$ for $X/H = 6$ to compare the velocity field calculated with and without the assumption of symmetry.

The symmetry of the current flow is evident from a number of independent measurements: chemiluminescence image (i.e., flame emissions without laser excitation), measured OH number densities,[13] and a comparison of velocity measurements with and without the assumption of symmetry for the plane located at $Z/D = \pm 1.0$. A chemiluminescence image of the flow obtained for the measurement region is presented in Fig. 9a. The highest signal occurs in two regions located on either side of the tunnel test-section center line. A graph of the signal intensity variation across the image is presented in Fig. 9b. It can be seen in the transverse variation that the peak signal value is located symmetrically about the test-section center line.

For the plane $Z/D = \pm 1.0$, the velocity field was calculated in three different ways: 1) assuming symmetry from direction i, 2) assuming symmetry from direction j, and 3) without assuming symmetry. Sample transverse variation profiles for streamwise velocity (U) at $X/H = 6$ are presented in Fig. 10. For the flow regions with the lowest uncertainties, i.e., the high-velocity regions at $X/H \sim 2$–2.5, the peak velocities occur symmetrically about the tunnel center line. The difference between the transverse profiles increases as the velocities decrease toward the tunnel center. However, at both locations the differences are within the uncertainty limits for the measurements. It appears that any errors introduced by the assumption of symmetry are smaller than the measurement uncertainties due to other factors.

The measured velocity field for the planes located at $Z/D = \pm 1.0, 0.0, +0.5, +1.0$, and $+2.0$ are presented in the form of streamwise velocity contours and vector fields in Fig. 11. The measured flowfield contains approximately 23,000 points. The resolution of these measurements (i.e., point to point spacing) is 200 μm. To simplify visualization of the flow structure, only every eighth point in the streamwise direction and every fourth point in the transverse direction has been displayed in the vector plots.

It can be seen in the velocity vector fields for all Z/D locations that the transverse velocity components are very small compared to the streamwise components. For the measurement plane $Z/D = \pm 1.0$, the flow is observed to turn in toward the center in the transverse region from $Y/H = 0.4$ to 1.6 on either side of the test-section center. This flow structure is visible to varying extents in the planes located at $Z/D = 0.0, 0.5$, and $+1.0$ in Fig. 11; however, the turning of the flow is visible most clearly at $Z/D = \pm 1.0$.

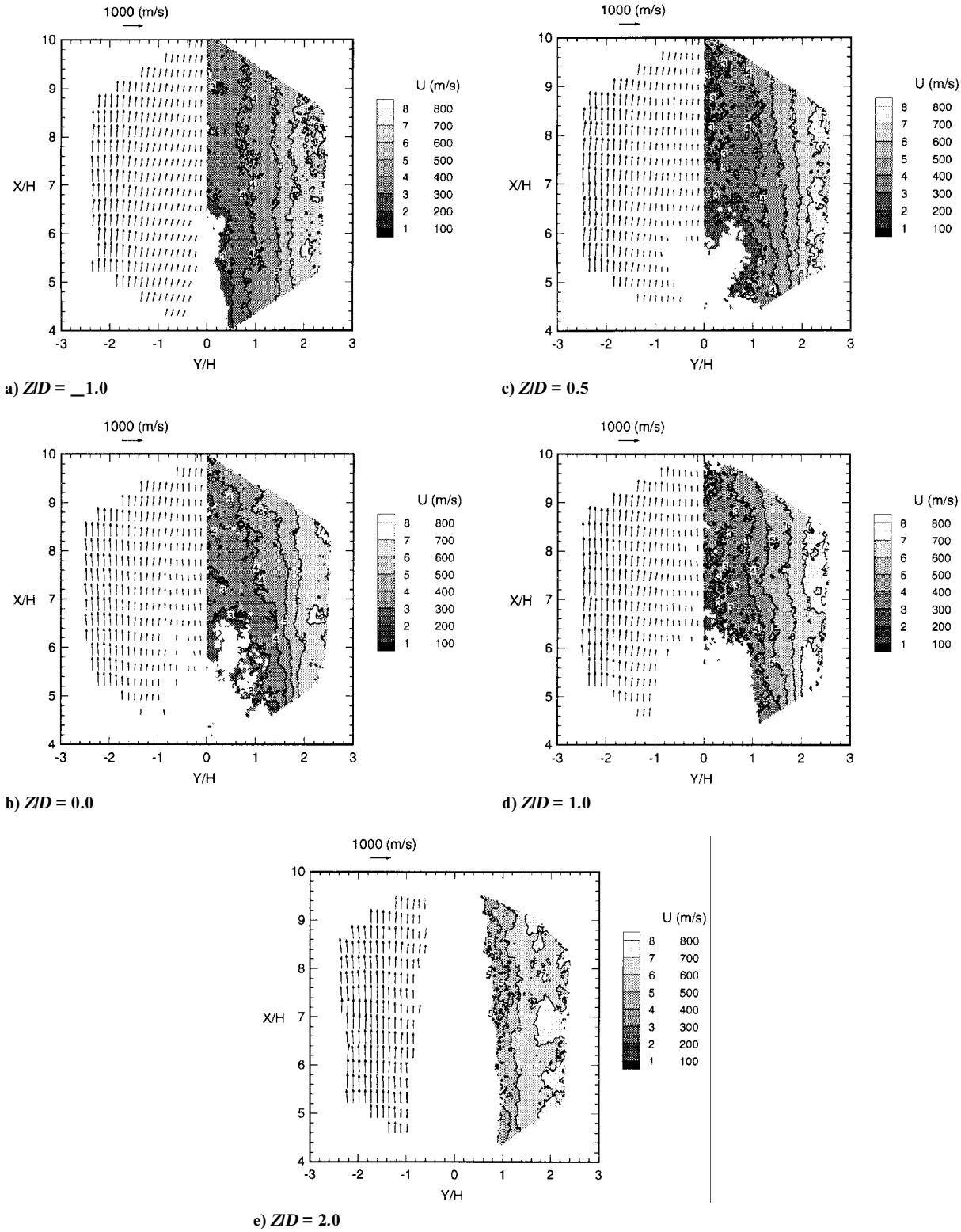

Fig. 11 Measured velocity vector field and axial velocity contours.

This pattern can partially be attributed to higher transverse velocity components at $Z/D = -1.0$ because this plane is located well below the injector for $4.0 < X/H < 10.0$. It can be seen that at $Z/D = 2.0$, because of the absence of signal, it is not possible to determine velocities in the flow center; this behavior is consistent with the fluorescence pattern displayed in Fig. 7.

Another consistent feature for all of the measurement planes is the increase in the streamwise component with increasing Y/H. This behavior is attributable to the formation of flame-holding recirculation regions in the region below the injected hydrogen. The higher streamwise components found at $Y/H \sim 2$–2.5 are associated with the main airflow. At any X/H location, the smallest streamwise component occurs at the center ($Y/H = 0$). As Y/H increases, the streamwise component increases.

The maximum streamwise component occurs for Y/H ranging from 2 to 2.5. The maximum streamwise component is approximately 700 m/s for the planes $Z/D = -1.0$, 0.0. This maximum value increases slightly up to 800 m/s for the planes $Z/D = 0.5$, 1.0, and 2.0. The uncertainties are estimated to be 6–8% in this region. Near the center of the flow ($Y/H = 0$), the streamwise component increases from about 200 m/s to 400 m/s (with an uncertainty of up to 20%) with increasing X/H.

Currently work is in progress for a full three-dimensional numerical simulation using SPARK, a CFD code with a finite-rate kinetic mechanism. However, the velocity distribution is consistent with the expected flow behavior. The main airstream is blocked by the ramp and the recirculation region formed downstream of the ramp. This results in a low velocity region at the tunnel center. Sufficiently far downstream, the main airstream turns in toward the tunnel center, forming a wake-like structure as observed in the measurements. Because the measurement planes are located well downstream and are below the injected jet for the X/H locations of the measurement region the flow velocities are less than the nominal values presented in Table 1. A one-dimensional analysis predicts that for the current conditions a thermally choked flow would approach a velocity of 900 m/s (Ref. 12). The measurement technique reported here can measure only two-dimensional velocity components within the measurement plane; therefore, the maximum axial flow velocities are consistent with the results of the one-dimensional analysis.

Summary and Conclusions

An application of Doppler-shifted OH PLIF velocity measurement to combusting supersonic flow has been demonstrated. Velocity measurements have been made for a reacting flowfield using an unswept ramp fuel injector in a Mach 2 scramjet combustor. The Doppler-shifted line center for an OH absorption line is determined by recording the broadband fluorescence emission while a narrow linewidth, tunable doubled-dye laser source is scanned through an OH absorption line. A counterpropagating beam approach has been used to eliminate impact shifts.

The velocity field has been measured in five planes, oriented parallel to the injector base wall, in the region 4–10 ramp heights downstream of the injector base. In this region, the measured spreading (transverse) component of the velocity field is small compared to the streamwise component. The maximum streamwise component is approximately 700–800 m/s and occurs at about 2–2.4 ramp heights on either side of the center line.

These measurements provide a quantitative, spatially complete velocity data set with a pixel-to-pixel spatial resolution of 200 μm for five distinct planes. The uncertainty of these measurements depends on OH signal level and velocity magnitude, with a typical uncertainty of $\pm$6–8% in the high velocity regions and $\pm$20–30% in the low-velocity, low-signal region at the combustor center.

These measurements represent the first successful application of a Doppler-shifted OH LIF velocimetry technique in the University of Virginia Aerospace Research Laboratory supersonic combustion tunnel. These results provide a velocity flowfield data set that can be used, together with OH absolute concentration and temperature data, for validation of CFD predictions.

Acknowledgments

This research was sponsored by NASA Grant NAG-1-795 from Langley Research Center, G. B. Northam, Technical Monitor. The tunnel operation for the velocity measurement experiments was partially supported by NASA Grant NAG-3-1518 from Lewis Research Center, Scott Thomas, Technical Monitor. The loan of the laser frequency stabilizer by R. J. Exton of NASA Langley Research Center is gratefully acknowledged.

References

[1]Northam, G. B., Greenberg, I., Byington, C. S., and Capriotti, D. P., "Evaluation of Parallel Injector Configurations for Mach 2 Combustion," *Journal of Propulsion and Power*, Vol. 8, No. 2, 1992, pp. 491–499.

[2]Drummond, J. P., Carpenter, M. H., and Riggins, D. W., "Mixing and Mixing Enhancement in Supersonic Reacting Flowfields," *High-Speed Flight Propulsion Systems*, edited by S. N. B. Murthy and E. T. Curran, Vol. 137, Progress in Astronautics and Aeronautics, AIAA, Washington, DC, 1991, pp. 383–455.

[3]Chinitz, W., Erdos, J. I., Rizkalla, O., Anderson, G. Y., and Bushnell, D. M., "Facility Opportunities and Associated Stream Chemistry Considerations for Hypersonic Air-Breathing Propulsion," *Journal of Propulsion and Power*, Vol. 10, No. 1, 1994, pp. 6–17.

[4]Krauss, R. H., and McDaniel, J. C., "A Clean Air Continuous Flow Propulsion Facility," AIAA Paper 92-3912, July 1992.

[5]Krothapalli, A., Shih, C., and Lourenco, L., "The Near Wake of a Circular Cylinder at $0.3 < M_\infty < 0.6$: A PIV Study," AIAA Paper 94-0663, Jan. 1994.

[6]Cho, Y. C., McLachlan, B. G., and Park, H., "Digital Image Velocimetry Applied to Determine Instantaneous Velocity Fields of A Moving Plate Wake," AIAA Paper 94-0046, Jan. 1994.

[7]Maurice, M. S., "A Method to Quantify and Correct Particle Velocity Bias in Laser Velocimetry Measurements," AIAA Paper 92-0764, Jan. 1992.

[8]Klavuhn, K. G., "Spatially-Resolved Velocity Measurements in Steady, High-Speed, Reacting Flows Using Laser-Induced OH Fluorescence," Ph.D. Dissertation, Dept. of Mechanical and Aerospace Engineering, Univ. of Virginia, Charlottesville, VA, May 1994.

[9]Klavuhn, K. G., Gauba, G., and McDaniel, J. C., "OH Laser-Induced Fluorescence Velocimetry Technique for Steady, High-Speed, Reacting Flows," *Journal of Propulsion and Power*, Vol. 10, No. 6, 1994, pp. 787–797.

[10]Krauss, R. H., McDaniel, J. C., Scott, J. E., Whitehurst, R. B. III, Segal, C., Mahoney, G. T., and Childers, J. M. IV, "Unique, Clean-Air, Continuous-Flow, High-Stagnation-Temperature Facility for Supersonic Combustion Research," AIAA Paper 88-3059, July 1988.

[11]Krauss, R. H., Whitehurst, R. B. III, Abbitt, J. D. III, Segal, C., and McDaniel, J. C., "Initial Supersonic Combustion Facility Measurements," AIAA Paper 89-2462, July 1989.

[12]McDaniel, J. C., Gauba, G., Quagliaroli, T. M., Grinstead, J. H., Laufer, G., Krauss, R. H., Whitehurst, R. B., and Victor, K. G., "Combustion of Hydrogen in Mach 2 Air Using an Unswept Ramp Fuel Injector: A Test Case for CFD Validation," AIAA Paper 94-2521, June 1994.

[13]Quagliaroli, T. M., Grinstead, J. H., Krauss, R. H., Laufer, G., Whitehurst, R. B., and McDaniel, J. C., "Planar OH Density and Apparent Temperature Measurements in a Supersonic Combustion Flow," AIAA Paper 95-0512, Jan. 1995.

K. Kailasanath
Associate Editor